Chinese Chemical Letters 35 (2024) 109694

Contents lists available at ScienceDirect

Chinese Chemical Letters

journal homepage: www.elsevier.com/locate/cclet

# Quantum dots boost large-view NIR-II imaging with high fidelity for fluorescence-guided tumor surgery

Biao Huang[a,1], Tao Tang[a,1], Fushou Liu[a], Shi-Hui Chen[a], Zhi-Ling Zhang[a], Mingxi Zhang[b], Ran Cui[a,*]

[a] College of Chemistry and Molecular Sciences, Wuhan University, Wuhan 430072, China
[b] State Key Laboratory of Advanced Technology for Materials Synthesis and Processing, Wuhan University of Technology, Wuhan 430070, China

ARTICLE INFO

*Article history:*
Received 20 November 2023
Revised 15 February 2024
Accepted 27 February 2024
Available online 6 March 2024

*Keywords:*
NIR-II imaging
Fluorescence-guided surgery
Quantum dots
Light-emitting diode
Tumor imaging

ABSTRACT

Owing to the high spatiotemporal resolution, the second near-infrared (NIR-II) imaging window can provide high imaging contrast with diminished tissue autofluorescence and suppressed photon scattering to pinpoint the locations for tumor surgery. Due to the unique optical properties and excellent fluorescence performance, quantum dots (QDs) are regarded as ideal nanoprobes for fluorescence-guided surgery (FGS). Moreover, QDs can be excited by a variety of light sources owing to the continuous and wide absorption ranges. Herein, light-emitting diode (LED) was used as the excitation source of QDs-based nanoprobes to realize FGS of tumor with high resolution. Since the LED light could irradiate a large region with consistent light intensity, signal distortion at the edge of imaging field was avoided. The signal intensity of the view edges under LED excitation can be improved by about 5 times compared to laser excitation. Therefore, more micro-vessels and smaller tumors ($V_{tumor}$ < 5 $mm^2$) could be detected, thus providing more precise guidance for tumor resection surgery.



Fluorescence imaging has emerged as a valuable intraoperative imaging technique that bridges the gap between preoperative imaging and the actual surgical procedure. It offers several advantages, including high resolution, high sensitivity, and the absence of ionizing radiation [1–6]. However, the presence of biological tissues significantly hampers photon penetration and leads to autofluorescence interference, which can greatly impact the effectiveness of fluorescence-guided surgery (FGS) [7–9]. Imaging in the second near-infrared region (NIR-II, 1000-1700 nm) can significantly reduce the interference of photon scattering and autofluorescence to provide deep tissue penetration and high-contrast imaging *in vivo* [10–12]. In recent years, a series of NIR-II probes, such as quantum dots (QDs) [13–16], organic small molecular dyes, polymer dots, and rare earth nanomaterials, have been developed to localize specific regions within the body and guide the subsequent surgery in a real-time manner [17–23].

Attributed to the unique optical properties such as wide absorption ranges, multiple emissions by unitary excitation for multicolor labeling, and high photostability allowing for long-duration imaging, QDs have shown great potential in FGS [24–26]. However, the inherent limitations of some NIR-II QDs, such as low absorption and unsatisfactory quantum yield in the NIR-II region, have already become the bottleneck to obtain higher contrast and spatiotemporal resolution imaging *in vivo*, greatly hindering their further applications in the FGS [27–29]. Notably, QDs usually possess higher absorption in the visible region (400–700 nm) than that in NIR window [30,31]. Therefore, visible lights can theoretically excite the stronger fluorescence of QDs to provide better imaging performance than NIR light sources.

In contrast to a typical laser beam with a Gaussian point spread function (PSF) and non-uniform light distribution, a light-emitting diode (LED) integrates multiple point light sources, which can provide a wide imaging field without signal distortion [32]. In this work, the white LED was used as the excitation for the FGS of tumors. Because of the higher absorption of QDs in the visible region, the LED light significantly improved the fluorescence intensity (1.5–2.5 times) and increased the penetration depth (~1 mm) compared to the 808 nm laser at the same optical power density. Due to the fluorescence enhancement of QDs under LED excitation, the signal-to-background ratio (SBR) and resolution of *in vivo* imaging were significantly improved. Some faint signals such as micro-vessels and micro tumor lesions can be clearly visualized to provide more detailed information for surgical operations with LED excitation. Since the LED light could irradiate a large region with

* Corresponding author.
*E-mail address:* cuiran@whu.edu.cn (R. Cui).
[1] These authors contributed equally to this work.

https://doi.org/10.1016/j.cclet.2024.109694
1001-8417/

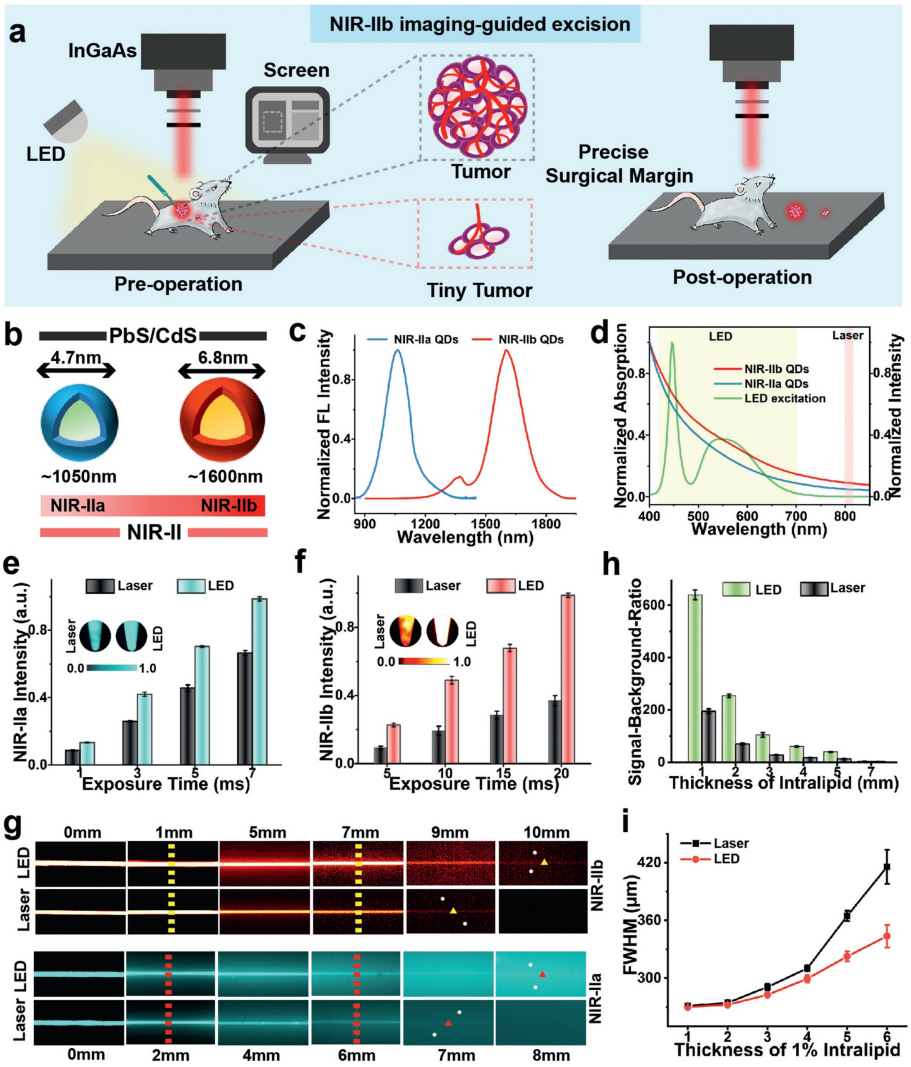


**Fig. 1.** (a) Illustration of LED light as the excitation source for NIR-IIb imaging-guided tumor resection surgery. (b) Illustration of NIR-IIa and NIR-IIb PbS/CdS QDs. (c) The fluorescence emission spectra of NIR-IIa QDs (blue curve) and NIR-IIb QDs (red curve). (d) The absorption spectra of NIR-IIa QDs (blue curve), NIR-IIb QDs (red curve), and emission spectrum of LED (green curve). (e) Fluorescence intensity analysis of NIR-IIa probes excited by LED or laser at different exposure times. (f) Fluorescence intensity analysis of NIR-IIb probes excited by LED or laser at different exposure times. (g) Fluorescence images of capillaries filled with NIR-IIb probes and NIR-IIa probes covered by 1% intralipid with varying depths under the excitation of LED or laser. The yellow and red triangle is the region of interest (ROI) of the capillary and the white circle is the ROI of the background. (h) Signal-to-background ratio of NIR-IIb imaging covered by varying depth 1% intralipid with the excitation of LED or laser. (i) The FWHM of Gauss fitted intensity data of NIR-IIa imaging of capillaries covered by varying depth 1% intralipid with the excitation of LED or laser. $n = 3$ independent samples (e, f, h, i).

consistent light intensity, signal distortion at the edge of the imaging field was avoided, which further improved the accuracy during the FGS. Overall, this work provided new perspectives for improving the *in vivo* imaging performance, providing a new direction for the development of new image-guided surgery.

Currently, the NIR lasers have been used as excitation sources for fluorescence surgical navigation systems, but the relatively low absorption of QDs in the NIR region greatly affects the *in vivo* imaging performance and immensely hinders their applications in FGS [33-36]. In this work, we focused on optimizing the excitation source which is another key of imaging processes. The white LED light was chosen as the excitation to promote the imaging performance of NIR-II QDs for imaging-guided tumor surgery (Fig. 1a).

To systematically compare the imaging performance of QDs under LED or NIR laser (808 nm) excitation, the commercial visible (white LED) and NIR (808 nm laser) light sources were used to study the influence of excitation wavelength on the imaging performance of two kinds of PbS/CdS QDs. These two kinds of QDs, emitting in ~1050 nm (in NIR-IIa region) and ~1600 nm (in NIR-IIb region) respectively (Figs. 1b and c), were synthesized according to our previous work (see Supporting information for details) [25]. To compare the fluorescence intensity of QDs excited by LED or laser, the NIR-IIb, and NIR-IIa PbS/CdS QDs were imaged under a NIR-II imaging system. As shown in Figs. 1e and f, the LED group showed stronger fluorescence signals compared to the laser group. According to the fluorescence intensity analysis of the images, the LED excitation evidently increased the fluorescence intensity of NIR-IIa (~1.5 times) and NIR-IIb QDs (~2.5 times) (Figs. 1e and f). The enhancement of the imaging performance may be caused by higher absorption of QDs in the visible region. The absorption of two kinds of PbS/CdS QDs in the visible region (400-700 nm) were both significantly higher than that in the NIR region (Fig. 1d). The emission wavelength of LED light mainly located in the visible region with two peaks intensity at ~445 nm and ~545 nm, which resulted in the enhancement of imaging performance of QDs.

The penetration depth and the SBR were also investigated to compare the imaging performance of QDs under LED or laser through phantom experiments [37–39]. The penetration depths of NIR-IIa (from 7 mm to 8 mm) and NIR-IIb (from 9 mm to 10 mm) QDs under LED excitation both increased by ~1 mm compared to

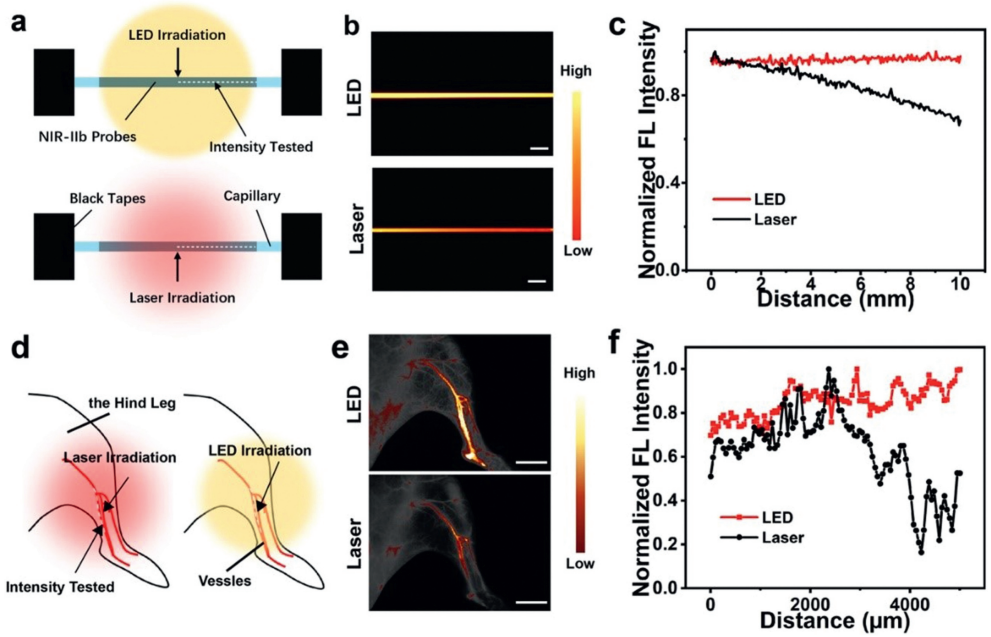


**Fig. 2.** (a) Schematic illustration of signal uniformity *ex vivo* for homogeneous illumination of LED and inhomogeneous illumination of the laser. (b) Fluorescence images of capillaries filled with NIR-IIb probes under LED (top) and laser (bottom) excitation. The imaging region is according to the dashed line in panel (a). Scale bar: 1 mm. (c) Intensity profiles along the capillary in panel (b) with NIR-IIb imaging under LED and laser excitation. (d) Schematic illustration of signal uniformity *in vivo* under LED and laser excitation. (e) Fluorescence images of the mouse hind limb in the NIR-IIb window under LED (top) and laser (bottom) excitation. Scale bar: 5 mm. (f) Intensity profiles along the vessels of mouse hind limb in (d).

the laser group (Fig. 1g). In addition, by analyzing the signal intensity of the capillary loading with QDs and the background, the LED group showed a higher imaging SBR than the laser group (Fig. 1h and Fig. S1 in Supporting information). In the NIR-IIb imaging window, the SBR of imaging at a depth of 1 mm in the intralipid solution reached 640.2 under LED excitation, which was about 3.3 times that of the laser group (SBR = 195.4) (Fig. S2a in Supporting information). When the depth increased to 7 mm, the SBR of imaging with LED excitation was 4.6, still approximately 70% higher than the SBR achieved under laser excitation (SBR = 2.6) (Fig. S2b in Supporting information).

To compare the imaging resolution between LED and laser excitation, the full width at half maximum (FWHM) was calculated according to the cross-sectional intensity profiles of the capillary. In the NIR-IIa window, when the imaging depth in intralipid was 2 mm, the LED group (273.9 μm) presented a similar FWHM as the laser group (274.5 μm) (Fig. S3a in Supporting information). However, as the imaging depth increased, the FWHM of the laser group increased dramatically (Fig. 1i). When the depth reached 6 mm, the FWHM of the LED group was 341.7 μm (Fig. S3b in Supporting information), which was 16.7% lower than that of the laser group (415.7 μm). Similarly, in the NIR-IIb window, the LED excitation also displayed lower FWHM (Fig. S4 in Supporting information), indicating that LED excitation could achieve higher resolution in deep penetration imaging. Since NIR-II QDs have higher absorption in the visible light region than in the NIR-II region, the visible light excitation can significantly improve the fluorescence intensity and penetration depth of NIR-II QDs, providing higher SBR and imaging resolution. Thus, LED has the potential as an ideal excitation source to improve imaging resolution and contrast for the QDs in the application in FGS.

In general, the normal laser beam obeys the Gaussian point spread function (GSF). Therefore, the intensity is expected to decrease gradually from the irradiation center to the surrounding areas, which may inevitably cause signal distortion at the border of the imaging field, especially during deep tissue and wide-field imaging *in vivo* [40–42]. As the schematic illustration shown in Fig. 2a, the intensity distribution of a capillary filled with NIR-IIb QDs solutions in NIR-II imaging with LED and the NIR laser were analyzed respectively. The intensity distribution along the capillary displayed a uniform pattern under LED excitation (Fig. 2b). In contrast, due to the inhomogeneous illumination of NIR lasers, the fluorescence intensity decreased by approximately 30% at the position 10 mm away from the laser radiation center (Fig. 2c). The above results confirmed that LED light source could provide a broader field of view with consistent light intensity for imaging than laser source.

Subsequently, *in vivo* imaging for hindlimb vessels was performed to verify the signal distortion under different excitation sources (Fig. 2d). When the laser is used as the imaging light source, the blood vessels in the mouse's legs show a strong signal in the center and a weak signal at the borders, with an intensity differential of up to 80% (Figs. 2e and f), which indicated that signal distortion occurred under laser radiation during *in vivo* imaging. In contrast, employing LED as an excitation source of QDs on the same mouse provided an expended image with uniform intensity (Figs. 2e and f), which may be a superior alternative for more precise guidance for FGS.

Iatrogenic injury of important structures is common in cancer surgery, so providing more information about tissue structures can help surgeons improve the accuracy and quality of operations [43–45]. To avoid damage to normal tissue and severe intraoperative bleeding, the identification and localization of vessels are essential during cancer surgery. In the whole-body image of the left side of the mouse shown in Fig. 3a, more signals from vessels were detected because of the higher fluorescence intensity of the probes with LED excitation. The statistics of vessels in the right limb of the mice showed that the average number of vessels detected by imaging with LED excitation was ~175 (Fig. 3b), almost twice that of the laser group (Fig. 3c). The size distribution of 100 vessels also showed that 66% of the vessels detected under LED excitation were in size range of 0-200 μm, and 25% were smaller than 150 μm

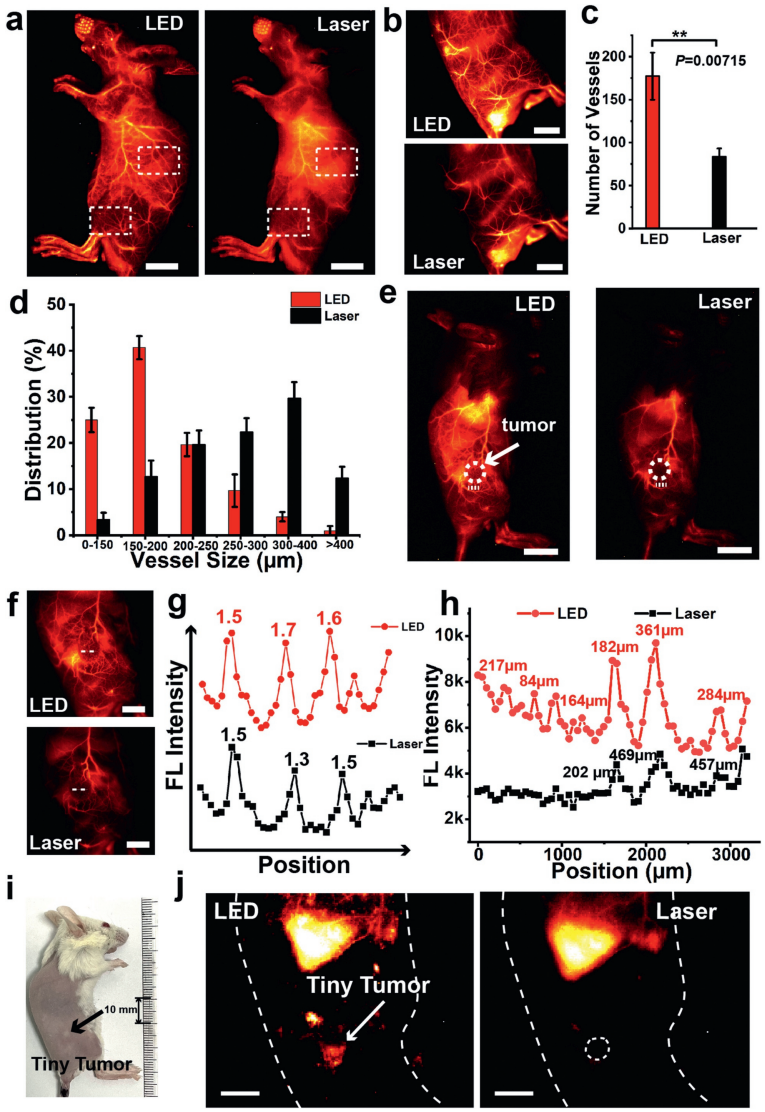


**Fig. 3.** (a) NIR-IIb images of healthy mice in left lateral position under the excitation of LED or laser. The dashed frame circled the region of interest. Scale bar: 10 mm. (b) NIR-IIb high-resolution images of healthy mice in right lateral position with high magnification (3× objective) under the excitation of LED or laser. Scale bar: 5 mm. (c) Average total vessels detected by NIR-IIb imaging with LED or laser excitation from (b). Statistical significance was calculated *via* a double-sample *t*-test. $n = 3$. ** $P < 0.05$. (d) Distribution of vessel sizes detected by high-resolution NIR-IIb imaging with LED or laser excitation investigated from (b). NIR-IIb images (e) and high-resolution images (f) of 4T1 tumor-bearing mice in right lateral position under the excitation of LED or laser. The dashed frame in (e) circled the location of tumors. Scale bar: 10 mm (e), 5 mm (f). (g) Intensity profiles and SBR of tumor vessels along the white line in (e). (h) Representative cross-sectional fluorescence intensity profiles of high magnification images along dashed lines of tumor micro-vessels by NIR-IIb imaging with LED or laser excitation. (i) Image of 4T1 tumor-bearing mouse. The black arrow points to the location of the tiny tumor ($d_{tumor} = 1.2$ mm). (j) NIR-IIb imaging for tiny tumors of mice with LED or laser excitation. Scale bar: 2 mm. $n = 3$ independent samples (c, d).

(Fig. 3d). In contrast, 84% of detected vessels were over the size of 200 μm with laser excitation. The above results indicated that some faint signals from tiny vessels could be enhanced by the increased fluorescence intensity with LED excitation, which may help to detect tiny vessels to provide more detailed information for surgical guidance.

The advantages of LED as a light source in imaging tumors, especially tiny tumors, were further investigated. The formation of tumor vessels is closely related to the development of cancer and requires special attention during surgeries [46,47]. Tumor angiography is one of the most important methods for imaging tumors. As shown in Figs. 3e and f, tumor vasculature networks can be observed with high clarity under LED excitation, and visualization of tumor-related vessels has higher imaging SBR (Fig. 3g). In addition, the cross-sectional intensity profiles of the tumors were analyzed to distinguish micro-vessels. As shown in Fig. 3h, LED excitation can detect more tumor micro-vessel signals with higher imaging resolution of the same 4T1 tumor-bearing mouse than laser excitation. In particular, the clinical imaging detection threshold for tumors is about 5–7 mm in diameter and the detection of tiny tumors (diameter < 2 mm), such as early or blood-borne metastasis tumors, remains a challenge owing to the sensitivity and specificity of current methods [48,49]. Here, the tiny tumor model (with a diameter less than 2 mm) was created to test sensitivity under LED excitation on the 3$^{rd}$ day after tumor cell implantation (Fig. 3i). When labeled with NIR-IIb PbS/CdS-RGD probes, the tumor (~1.2 mm in diameter) showed obvious signal enhancement under LED excitation, whereas no obvious tumor signal was observed under laser excitation (Fig. 3j). The above results indicated that LED excitation could significantly improve the *in vivo* imaging performance of NIR-II QDs, making it an ideal excitation source to provide more valuable information for tumor FGS.

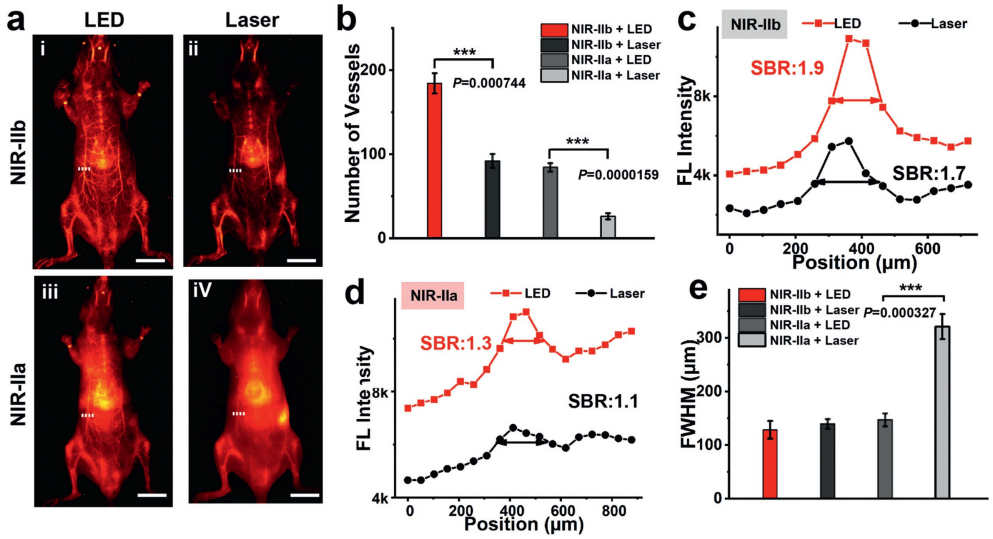


**Fig. 4.** (a) NIR-IIa and NIR-IIb imaging images of mice in the upright position under LED and laser excitation. NIR-IIa channel: 980 LP plus 1200 SP filters. NIR-IIb channel: 980 LP plus 1500 LP filters. Scale bar: 10 mm. (b) Average total vessels detected by NIR-IIa and NIR-IIb imaging with LED or laser excitation. Representative cross-sectional fluorescence intensity profiles of images along white dashed lines of vessels in panel (a) by NIR-IIb (c) and NIR-IIa (d) imaging. (e) The FWHM of Gauss fitted intensity data of NIR-IIa and NIR-IIb imaging of mouse vessels. Statistical significance was calculated *via* a double-sample *t*-test. $n = 3$. *** $P < 0.001$. $n = 3$ independent samples (b, e).

Currently, QDs emitting in the range of NIR-IIa account for the majority of NIR-II QDs, but the much lower imaging SBR and resolution compared with NIR-IIb QDs severely limit the guidance accuracy of NIR-IIa QDs in surgeries [50–52]. Meanwhile, there are still a few NIR-IIb QDs with sufficient brightness and stability to be used for FGS. Fortunately, LED excitation can significantly enhance the SBR and improve imaging resolution. Therefore, it was also promising to promote the *in vivo* imaging performance of NIR-II QDs.

To convincingly compare the imaging performance between NIR-IIa and NIR-IIb QDs with different excitation sources, the NIR-IIa and NIR-IIb probes were mixed in equal parts and then injected into the tail vein of the same mice to perform *in vivo* imaging. Attributed to the enhanced fluorescence signals from QDs under LED excitation, the imaging quality between the two windows was significantly promoted, more vessels could be visualized with higher clarity (Fig. 4a). According to the statistics of vessels detected under different imaging conditions, the number of detected vessels in the NIR-IIa imaging window with LED excitation was about 3 times that of laser excitation, and reached almost the same level as that in the NIR-IIb imaging under laser excitation (Fig. 4b). In addition, LED excitation markedly improved the SBR of in NIR-IIa and NIR-IIb imaging window by 18% and 11%, respectively (Figs. 4c and d). Moreover, the FWHM of the tested vessel in the NIR-IIa imaging window under LED excitation was significantly decreased, which was close to NIR-IIb imaging quality under laser excitation (Fig. 4e). Therefore, LED excitation could evidently improve the imaging performance of NIR-IIa QDs comparable to that of NIR-IIb QDs under laser excitation, which allowed a wider choice of NIR-II probes for the application in tumor FGS.

The potential application of PbS/CdS QDs under LED excitation in imaging-guided tumor resection was investigated using 4T1 tumor-bearing mouse models. Providing sufficient light intensity is conducive to smooth operations [53]. As shown in Fig. S5 (Supporting information), the NIR-II imaging system was equipped with LED light, which provided sufficient bright conditions for various surgical procedures without an additional light source. Before imaging-guided surgery, the NIR-IIb PbS/CdS QDs were modified with arginine-glycine-aspartate (RGD) peptide to construct the tumor-targeted nanoprobes (PbS/CdS-RGD) according to our previous work [47,54]. For long-time imaging during FGS, the photostability of probes was tested under LED irradiation. After continuous irradiation with LED for 2 h, the fluorescence intensity did not seriously decrease (Figs. S6 and S7 in Supporting information), indicating that the LED did not significantly affect the photostability of NIR-IIb and NIR-IIa probes and helped to avoid signal distortion caused by fluorescence attenuation during operations.

To determine the optimal imaging time window for FGS, tumor-bearing mice were imaged at different time points. As shown in Figs. 5a and b, the signal of the tumor gradually increased with time, indicating the good tumor-targeting ability of PbS/CdS-RGD probes. In addition, the imaging SBR of tumors under LED excitation was significantly higher than that of laser (Fig. 5c), peaking at 8 h after injection. Therefore, the ideal imaging window for surgery was set within 4–8 h after injection. As shown in Movie S1 (Supporting information), NIR-IIb imaging with LED excitation outlined the margin of the tumor. Combined with visual inspection, the resection surgery of the tumor was successfully completed. After surgery, there were no obvious fluorescent signals at the tumor site (Fig. 5d), indicating that the primary tumor was successfully removed.

In summary, we developed an optimized large-view NIR-II imaging system equipped with LED excitation as the excitation source of QD-based probes and realized precise fluorescence-guided surgery of tumors. The home-built LED-excited NIR-II imaging system increased the contrast (NIR-IIa ~1.5 times and NIR-IIb ~2.5 times) and penetration depth, which significantly improved the imaging quality in the NIR-II window. Consistent irradiation of LED light considerably expanded the effective imaging area by avoiding the signal distortion with a ~5-fold increase at the edge of the imaging view. Additionally, the number of micro-vessels detected in the NIR-IIa window under LED excitation *in vivo* was nearly equal to that found in the NIR-IIb window under laser excitation. Moreover, tiny tumors (~1.2 mm in diameter) can be detected, providing a consistent wide field of view with more precise guidance for tumor resection surgery. Our results open up new avenues for large-view NIR-II imaging while avoiding signal distortion, enabling a wider choice of NIR-II probes for application in tumor FGS.

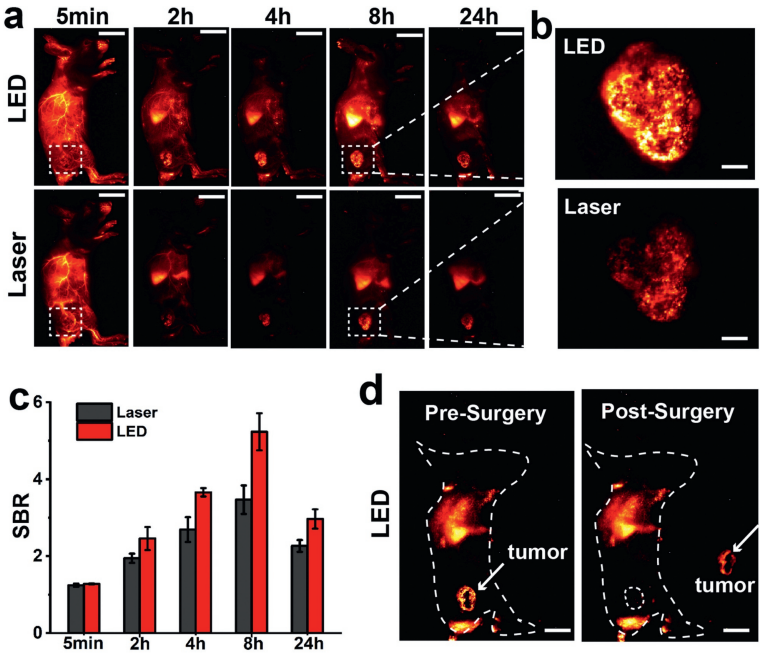


**Fig. 5.** (a) NIR-IIb imaging for tumor-bearing mice at different time points. Scale bar: 10 mm. (b) NIR-IIb imaging for tumor-bearing mice at 8 h post-injection of PbS/CdS-RGD probes. Scale bar: 1 mm. (c) SBR of NIR-IIb imaging for tumor *versus* time. (d) NIR-IIb imaging of mice pre-and post-surgery. Scale bar: 10 mm. $n = 3$ independent samples (c).

## Ethics statement

Ethical approval of this study was obtained from the Animal Ethics Committee of the School and Hospital of Stomatology, Wuhan University (approval number: S07920070E). All animal experimental procedures were performed following the Regulations for the Administration of Affairs Concerning Experimental Animals approved by the State Council of the People's Republic of China.

## Declaration of competing interest

The authors declare that they have no known competing financial interests or personal relationships that could have appeared to influence the work reported in this paper.

## Acknowledgments

This work was supported by the National Natural Science Foundation of China grant (Nos. 22174105 and 21974104), and the National Key R&D Program of China (No. 2020YFA0908800). We thank the Large-scale Instrument and Equipment Sharing Foundation of Wuhan University.

## Supplementary materials

Supplementary material associated with this article can be found, in the online version, at doi:10.1016/j.cclet.2024.109694.

## References

[1] Z. Hu, C. Fang, B. Li, et al., Nat. Biomed. Eng. 4 (2020) 259–271.
[2] J.S.D. Mieog, F.B. Achterberg, A. Zlitni, et al., Nat. Rev. Clin. Oncol. 19 (2022) 9–22.
[3] F. Wang, L. Qu, F. Ren, et al., Proc. Natl. Acad. Sci. U. S. A. 119 (2022) e2123111119.
[4] S. Hernot, L. Manen, P. Debie, et al., Lancet Oncol. 20 (2019) 354–367.
[5] Y.Y. Duo, L. Zhao, Z.G. Wang, et al., J. Anal. Test. 7 (2023) 245–259.
[6] Y. Yang, D. Liu, Z. He, et al., Adv. Healthcare Mater. 12 (2023) 2300434.
[7] C. Li, Y. Pang, Y. Xu, et al., Chem. Soc. Rev. 52 (2023) 4392–4442.
[8] S. He, J. Song, J. Qu, et al., Chem. Soc. Rev. 47 (2018) 4258–4278.
[9] X. Song, R. Wang, J. Gao, et al., Chin. Chem. Lett. 33 (2022) 1567–1571.
[10] Y. Chen, P. Pei, Z. Lei, et al., Angew. Chem. Int. Ed. 60 (2021) 15809–15815.
[11] H. Zhang, C. Sun, L. Sun, et al., Angew. Chem. Int. Ed. 61 (2022) e202203851.
[12] J. Zheng, S.H. Chen, B. Huang, et al., Chin. Chem. Lett. 35 (2024) 108460.
[13] R. Tian, H. Ma, S. Zhu, et al., Adv. Mater. 32 (2020) 1907365.
[14] P. Wang, J. Li, M. Wei, et al., Biomaterials 287 (2022) 121636.
[15] H.L. Xu, J.J. Yang, D.L. Zhuge, et al., Adv. Healthcare Mater. 7 (2018) 1701130.
[16] S. Qu, Q. Jia, Z. Li, et al., Sci. Bull. 67 (2022) 1274–1283.
[17] C. Sun, X. Sun, P. Pei, et al., Adv. Funct. Mater. 31 (2021) 2100656.
[18] H. Zhou, S. Li, X. Zeng, et al., Chin. Chem. Lett. 31 (2020) 1382–1386.
[19] X. Zhou, Q. Liu, W. Yuan, et al., Adv. Sci. 8 (2021) 2000441.
[20] P. Wang, Y. Fan, L. Lu, et al., Nat. Commun. 9 (2018) 2898.
[21] D. Li, S. He, Y. Wu, et al., Adv. Sci. 6 (2019) 1902042.
[22] J. Jin, L. Yang, F. Chen, et al., Interdiscip. Mater. 1 (2022) 471–494.
[23] D. Liu, Z. He, Y. Zhao, et al., J. Am. Chem. Soc. 143 (2021) 17136–17143.
[24] Q. Wen, Y. Zhang, C. Li, et al., Angew. Chem. Int. Ed. 58 (2019) 11001–11006.
[25] G.T. Yu, M.Y. Luo, H. Li, et al., ACS Nano 13 (2019) 12830–12839.
[26] Z. Feng, T. Tang, T. Wu, et al., Light: Sci. Appl. 10 (2021) 197.
[27] W. Zhang, T. Chen, L. Su, et al., Anal. Chem. 92 (2020) 6094–6102.
[28] H. Yang, R. Li, Y. Zhang, et al., J. Am. Chem. Soc. 143 (2021) 2601–2607.
[29] Z.Y. Liu, A.A. Liu, H. Fu, et al., J. Am. Chem. Soc. 143 (2021) 12867–12877.
[30] J. Zhang, A. Bifulco, P. Amato, et al., J. Colloid Interf. Sci. 638 (2023) 193–219.
[31] C. Mahajan, A. Sharma, A.K. Rath, ACS Appl. Mater. Interfaces 12 (2020) 49840–49848.
[32] L. Lu, B. Li, S. Ding, et al., Nat. Commun. 11 (2020) 4192.
[33] J. Liu, H. Rijckaert, M. Zeng, et al., Adv. Funct. Mater. 28 (2018) 1707365.
[34] Q. Liu, J. Tian, Y. Tian, et al., Acta Biomater 127 (2021) 287–297.
[35] S. Fan, S. Wang, C. Yang, et al., Adv. Optical Mater. 23 (2023) 2202945.
[36] N. Liu, X. Chen, X. Sun, et al., J. Nanobiotechnol 19 (2021) 113.
[37] A. Satpathy, W.T. Huang, M.H. Chan, et al., Adv. Optical Mater. 11 (2023) 2300321.
[38] Z. Feng, Y. Li, S. Chen, et al., Nat. Commun. 14 (2023) 5017.
[39] B. Li, M. Zhao, J. Lin, et al., Chem. Soc. Rev. 51 (2022) 7692–7714.
[40] Y. Liu, Z. Zhou, F. Wang, et al., Nat. Commun. 12 (2021) 2019.
[41] C. Chen, B. Liu, Y. Liu, et al., Adv. Mater. 33 (2021) 2008847.
[42] S. Jia, J.C. Vaughan, X. Zhuang, Nat. Photonics 8 (2014) 302–306.
[43] M. Wei, J. Bai, X. Shen, et al., ACS Nano 17 (2023) 11345–11361.
[44] T. Pu, Y. Liu, Y. Pei, et al., ACS Appl. Mater. Interfaces 15 (2023) 32226–32239.
[45] Y. Wang, J. Nan, H. Ma, et al., Nano Lett. 23 (2023) 4039–4048.
[46] M. Wenes, M. Shang, M. Di Matteo, et al., Cell Metab. 24 (2016) 701–715.
[47] T. Tang, B. Huang, F. Liu, et al., Nanoscale 14 (2022) 7473–7479.
[48] N. Pashayan, P.D.P. Pharoah, Science 368 (2022) 589–590.
[49] J. Huang, X. Chen, Y. Jiang, et al., Nat. Mater. 21 (2022) 598–607.
[50] Y. Zhou, B. Huang, S.H. Chen, et al., Nano Res. 16 (2023) 2719–2727.
[51] A.M. Saeboe, A.Y. Nikiforov, R. Toufanian, et al., Nano Lett. 21 (2021) 3271–3279.
[52] Q. Ding, J. Zhao, H. Zhang, et al., Angew. Chem. Int. Ed. 61 (2022) e202210370.
[53] J.X. Sun, J.Z. Xu, Y. An, et al., J. Control. Release 353 (2023) 832–841.
[54] B. Huang, J. Hu, H. Li, et al., ACS Appl. Bio Mater. 3 (2020) 1636–1645.